Nanoscale

Accepted Manuscript

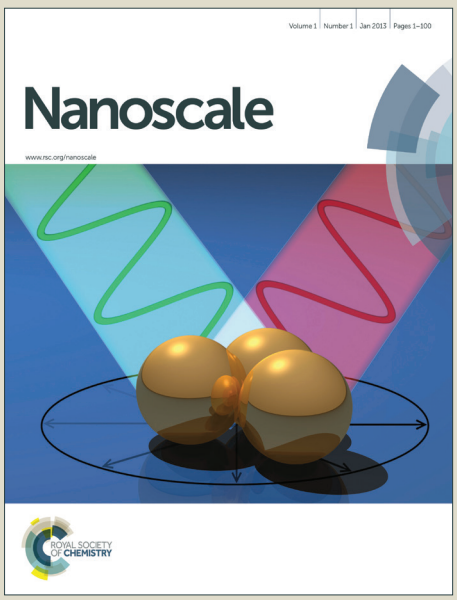

ROYAL SOCIETY OF CHEMISTRY

www.rsc.org/nanoscale

Journal Name

Dynamic Article Links ►

Cite this: DOI: 10.1039/c0xx00000x

www.rsc.org/xxxxxx

ARTICLE TYPE

Plasmonic nanorod arrays of two-segment dimer and coaxial cable with 1 nm gap for large field confinement and enhancement

Zi-Qiang Cheng,[a] Fan Nan,[a] Da-Jie Yang,[a] Yu-Ting Zhong,[a] Liang Ma,[a] Zhong-Hua Hao,[a] Li Zhou*[a] and Qu-Quan Wang*[ab]

Received (in XXX, XXX) Xth XXXXXXXXX 20XX, Accepted Xth XXXXXXXXX 20XX

DOI: 10.1039/b000000x

Seeking plasmonic nanostructures with large field confinement and enhancement is significant for photonic and electronic nanodevices with high sensitivity, reproducibility, and tunability. Here, we report the synthesis of plasmonic arrays composed by two-segment dimer nanorods and coaxial cable nanorods with ~1 nm gap insulated by self-assembled Raman molecule monolayer. The gap-induced plasmon coupling generates intense field in the gap region of dimer junction and cable interlayer. As a result, the longitudinal plasmon resonance of nanorod array with high tunability is obviously enhanced. Most interesting, the field enhancement of dimer nanorod arrays can be tuned by the length ratio L_1/L_2 of two segments, and the maximal enhancement appears at $L_1/L_2 = 1$. In that case, the two-photon luminescence (TPL) of dimer nanorod array and the Raman intensity in the dimer junction is enhanced by 27 and 30 times respectively under resonant excitation. In the same way, the Raman intensity in the gap region is enhanced 16 times for the coaxial cable nanorod arrays. The plasmonic nanorod arrays synthesized by the facile method, having tunable plasmon properties and large field enhancement, indicate an attractive pathway to the photonic nanodevices.

1. Introduction

Amplification of optical signals is greatly desired in many applications like sensing [1], molecule detecting and identification [2-4], optical information process [5,6], etc. Localized surface plasmon resonances (LSPRs) of metallic nanostructures could concentrate light energy into sub-wavelength nanoscale and lead to large electromagnetic field confinement and enhancement [7,8]. The spectral responses and spatial field distributions of LSPRs are greatly determined by the composition, shape, size and environment of metallic nanostructures, which provide LSPRs highly tailorability in the system of light-matter interaction [9,10]. Then, LSPR is considered as a powerful tool to realize the optical amplification and exhibit attractive potential in acting as building block in photonic nanodevices [11].

With the help of metallic nanostructure having unique LSPRs properties, many efforts have been devoted to improve the enhancement factor of optical signals and explore the extreme applications of plasmon, for example, single molecule detecting [12-14], nanolaser [15-17], etc. For seeking large field enhancement, target molecules are designed to locate in the surface of arbitrary and anisotropic nanoparticles, where the small curvature could produce large local field [18-20]. The inter-particle gap and junction is a more ideal position as hot spot because the inter-particle plasmon coupling could induce dramatic field confinement and enhancement compared with single nanoparticles [14,21]. Recently, the research has gone deep into the accurate controlling of the inter-particle distance from tens of nanometers to ~1 nm [22,23]. The plasmonic array with periodic hot spots is an ideal substrate and has been widely applied and studied [24-27]. Lithography fabrication can produce metallic arrayed nanostructures with highly controlled shape and size [28,29], then with highly tunable plasmon properties. At present, the fabrication of sub-10 nm gap is a challenge process for lithography [30,31]. The substrate of self-assembled nanoparticle array can be produced facilely, while lack of reproducibility and uniformity is a problem [32,33]. The electrodeposited metallic nanorod (NR) array with vertically aligned structures is an interesting substrate possessing tunable plasmonic resonance dependent on the rod-length and unique hot spot distribution induced by the inter-rod coupling [34-36]. Moreover, the post-treatment like lateral aggregation and deposition of nanoparticles on top could produce narrow gaps namely hot spots with intense field between the adjacent NR tips [37,38].

Surface-enhanced Raman scattering (SERS) and plasmon-enhanced luminescence are the representative examples of optical signal enhancement produced by plasmon [39-42]. For SERS application, the contribution of plasmon is determined by: i) the field enhancement factor near the metallic surface [19,43]; ii) the spatial overlap of the field hot spot and Raman molecule location [44]; iii) the resonance situation of plasmon wavelength and excitation light as well as Raman emission [29,45]. All these factors influence the sensitivity, reproducibility, and tunability of the SERS applications and thus the preparing of SERS substrate

is very important for the final detecting of Raman signal. However, for usual SERS application, the distribution of target Raman molecules is random on the substrate. The weight of effective Raman molecules located in hot spots with high enhancement as well as high SERS reproducibility is limited. Recently, many literatures have reported that using specific Raman-active molecules (thiol-group, DNA-anchored, etc.) [23,46,47] as both Raman tag and binding linker to assemble and synthesis metallic nanostructures with ultra-narrow and accurately controlled gap. These structures exhibit outstanding SERS performance because the target Raman molecules are almost all located in the gap, which generates a perfect spatial overlap with the intense and uniform field.

In this paper, we use two-step deposition method to prepare two-segment dimer NR arrays and coaxial cable NR arrays in the anodic aluminum oxide (AAO) template. Between the two depositions, a single layer thiol Raman molecules are self-assembled onto the uncovering surface of the 1st gold NRs (AuNRs). The two-step deposition produces an interior ~1 nm gap with large field confinement and enhancement in the junction of two-segment dimers as well as in the interlayer of coaxial cable. The method integrates the advantages of electrodeposited metallic NR array and molecule mediated self-assembly, which could produce sub-10 nm gap more effective than lithography route and fabricate periodic array beyond normal self-assembly. The optical responses of extinction spectra, two-photon luminescence (TPL) and Raman scattering are investigated to reveal the nature of plasmon enhancement and the dependent properties on the detail structural parameters. The studies in this paper are important for the fundamental understanding and photonic application of LSPRs.

2. Experimental Section

2.1 Preparing of AAO template

The high-order AAO used in this work was prepared through a two-step electrochemical anodization process, which is described elsewhere [48]. Anodization was carried out at a constant DC voltage of 40 V and the constant temperature 4 ℃ in a solution of 0.3 M $H_2C_2O_4$ for 4 h. After the first anodization step, the alumina layer was removed by wet chemical etching in a mixture of 1.8 wt% H_2CrO_4 and 6 wt% H_3PO_4 at 60 °C for 1 h. The sample was anodized for 2.5 h again at the same condition as the first anodization. The barrier layer of AAO templates was thinned stepwise with reducing potential at the end of the second anodization process.

2.2 Electrodepositing and functionalize of samples

The preparation procedures of the two-segment dimer NRs and coaxial cable NRs arrays within AAO template are illustrated schematically in Figure 1(a) and 4(a), respectively. Following the approach and ideas has been recently described in reference [49] and [50-53]. The Au (Ag) was electrodeposited in the nanochannels of AAO templates by alternating-current electrolysis (50 Hz, 7 V) in an electrolyte containing $HAuCl_4$ (0.01 M) and H_2SO_4 (0.1 M) ($AgNO_3$ (0.03 M) and H_2SO_4 (0.03 M)). Firstly, The Au was electrodeposited in the nanochannels of AAO templates and washed with distilled water. For coaxial cable Au@Ag NRs arrays, the pore diameter of AAO films with Au NRs filled was enlarged by a wet chemical etching in an aqueous solution of 5 wt% H_3PO_4 for 15 min at 35 °C. To chemically functionalize the structures, the entire film was then submerged into a 1 mM ethanol solution of 1,4-benzenedithiol (1,4-BDT) for 22 hours and then washed several times in ethanol to remove weakly bound molecules. The Raman molecules self-assembled on the tip and/or surface of Au NRs deposited in the pores. Then Au/Ag was deposited again after washing with ethanol. The 1,4-BDT molecules act as spacers, preventing the Au/Ag from touching each other. After deposited, the Al substrate was removed by using the mixture of HCl and $CuCl_2$ solution. The barrier layer was removed and the alumina matrix was partially etched to expose the tips of NRs by immersing the samples in a 5 wt% H_3PO_4 solution for 25 min at 35 °C. After partially etching aluminum, the back-end alumina serves as a SERS substrate.

2.3 Characterizations

The morphology and structures of the SERS substrates were characterized by using scanning electron microscopy (SEM, Hitachi S-4800), transmission electron microscope (TEM, JEOL 2010 HT), and high resolution TEM (HRTEM, JEOL 2010 FET). EDX analysis was performed on an EDAX instrument incorporated in the HRTEM. The extinction spectra were measured at room temperature using an Ultraviolet-visible-near infrared (UV-Vis-NIR) spectrophotometer (Varian Cary 5000) whit a *p*-polarized source, the incident angle was set at 70°.

2.4 SERS measurements

The SERS spectra were measured using a micro-Raman system (HORIBA Jobin Yvon LabRAM HR800) equipped with a thermoelectrically cooled CCD detector and in the normal way by laser beam irradiation perpendicular to the surface of the sample with vertical NRs A typical 785 nm wavelength diode laser coupled to a holographic notch filter was used to excite the samples. Scans were taken on an extended range (600–1650 cm^{-1}) with the excitation power of 100 mW, 10× microscope objective and the acquisition time of 10 s.

2.5 TPL measurements

The excitation source for TPL was a mode-locked Ti/sapphire pulsed laser (Mira 900, Coherent) with pulse width approximately 100 fs and a repetition rate of 76 MHz. The laser wavelength was fixed at 785 nm. The *p*-polarized light was obliquely incident to the samples. The TPL signals at room temperature were collected by a reflection measurement and recorded through spectrometry (Spectrapro 2500i, Acton) with a liquid-nitrogen-cooled charge-coupled device (SPEC-10, Princeton).

2.6 Simulations

The simulations were carried out by using 3D finite-difference time domain (FDTD) method with the software FDTD Solutions 8.6 (see detail in SI). The dielectric constant of gold and silver are taken from Johnson and Christy's article [54] and Palik's book [55]. The rod diameter d = 30 nm, the array period a = 100 nm, and the gap size Δ = 2 nm. The refractive index of AAO is 1.6 [42].

3. Results and Discussion

The two-step deposition method introduced here is a facile and effective way for making two-segment dimer NRs and coaxial cable NRs. We firstly demonstrate the preparing and performance of the dimer NR arrays. The detail fabrication procedure is shown in Fig. 1a. 1,4-BDT molecules were employed as the assembled insulators as well as the Raman probes, because of its ability to adsorb on gold or silver surfaces (with thiol groups) and its distinct Raman fingerprint. Through the process of adsorption and washing, a monolayer of 1,4-BDT molecules was assembled on the uncovered top end surface of the 1st AuNRs and then was confined in the dimer junction after the deposition of 2nd AuNRs. As the mouth-side of an AAO template shown in Figure 1b, the prepared AAO template possesses highly ordered nanopore arrays with an average diameter approximately 32 nm and a period (interpore distance) about 100 nm. For pursuing the high quality of optical spectra, the barrier layer of AAO was removed and the alumina matrix was partially etched to expose the NRs tips by immersing the samples in a 5 wt% H_3PO_4 solution for 25 min at 35 °C. Figures 1c show the etched back-side of the highly ordered nanopores filled with dimer AuNRs. The entire barrier layer has been removed and the network of dimer AuNRs is revealed. The tips of AuNRs protrude slightly above the alumina matrix, it can be seen that almost every pore of the alumina structure was filled. The ~28 nm average diameter of dimer AuNRs is a little smaller than that of pores shown in Fig. 1b, because the pore size at the mouth-side is larger compared with that at the back-side during the anodization [56]. The inset in Fig. 1c shows a ~1.3 nm gap separated by a monolayer 1,4-BDT molecules [57].

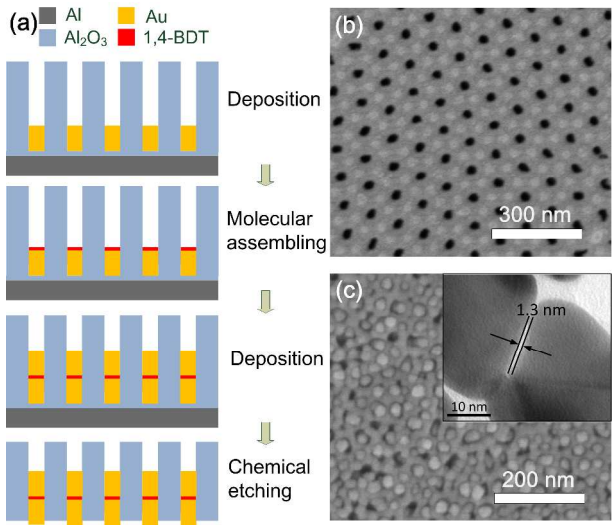

Fig. 1 (a) Schematic illustration for preparing two-segment dimer AuNR array. SEM images of (b) mouth-side of a AAO template and (c) etched back-side of a two-segment dimer AuNRs. The inset shows ~1.3 nm gap in a two-segment dimer AuNR.

The NR arrays exhibit more tunable and intense plasmon resonances compared with the individual NR due to the side-to-side coupling of the periodic structure [34-46]. Here, the end-to-end arrangement along the longitudinal direction of two-segment NRs would introduce a new coupling effect based on array structure. Due to the bonding of thiol group on the surface of Au and the specific configuration ways of molecules, the gap distance is near 1 nm [57]. Previous literatures show that the ultra-narrow gap of ~1 nm could introduce ultra strong fileld enhancement compared with the single nanoparticles [22,58]. Figure 2a compares the extinction spectra of the one-segment Au NR array and two-segment dimer Au NR arrays embedded in the AAO templates (the barrier layers were removed), which were recorded by using *p*-polarized source with the incident angle 70°. The extinction spectra have two characteristic bands due to the transverse (T-SPRs, at ~530 nm) and longitudinal (L-SPRs, at ~785 nm) surface plasmon resonances. For comparing the plasmon intensity, the L-SPR wavelengths of the two samples are set nearly same. It can be obviously seen that the L-SPR extinction intensity of two-segment dimer NRs shows greatly enhanced and much narrower in width. We speculate that the enhanced extinction corresponding to the enhanced plasmon resonances is caused by the end-to-end coupling induced intense field confined in the gap region of the dimer AuNR unit.

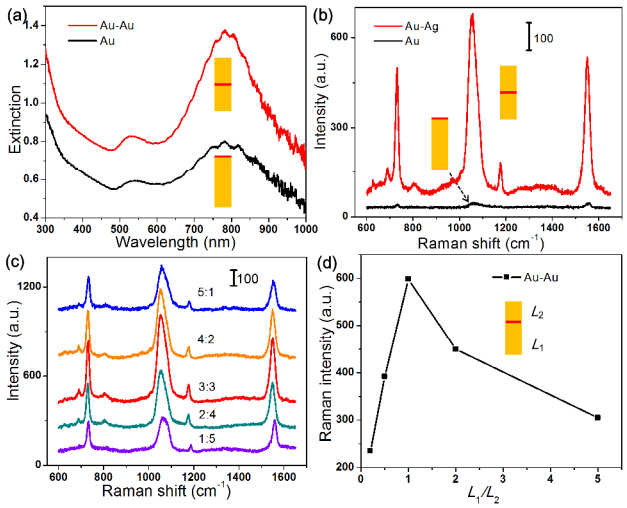

Fig. 2 (a) Extinction and (b) SERS spectra of one-segment and two-segment AuNRs arrays with1,4-BDT molecules adsorbed on the top end of Au NRs and confined in the junctions of two-segment dimer AuNRs, (c) SERS spectra of five two-segment dimer AuNR array samples with different length ratio L_1/L_2 of the two segment. The length ratio L_1/L_2 is 1:5, 2:4, 3:3, 4:2 and 5:1, respectively; (d) SERS intensity at 1067 cm^{-1} as a function of the length ratio L_1/L_2.

We firstly apply the SERS measurement to demonstrate the large local field enhancement. Figure 2b show the Raman spectra of the two-segment dimer array and the one-segment AuNR array. The excitation is a 785 nm laser and then resonates with the L-SPRs of both samples. In the micro-Raman system, the excitation light polarization is parallel to the short axis of NRs before objective lens. However, at the edge of lens with short focal length, part of the laser beam is refracted with a wide angle and irradiates the NRs at some angle, having a polarization component parallel to the long axis of NRs [59]. The tips of AuNR dimers were etched out for avoiding the obstruction of Raman signals by the barrier layer in AAO (see detail in Fig. S1). The four main peaks at 730 cm^{-1} (7a vibrational mode), 1067 cm^{-1} (combination of the phenyl ring breathing, CH in-plane bending, and CS stretching, ν1), 1180 cm^{-1} (CH bending, 9a mode), and 1556 cm^{-1} (phenyl ring stretching, 8a mode) agree well with the pattern of 1,4-BDT molecules reported in references [60-63]. The strongest peak at 1067 cm^{-1} is utilized to compare the SERS intensity. The SERS signal of the two-segment dimer array is approximation 30 times larger than that of one-segment

AuNR array. In our experiments, the adsorbed 1,4-BDT molecules are all located in the specific position (a monolayer with nearly same area in the junction of the dimer AuNRs or on the top end surface of the one-segment AuNRs) while the residual molecules on the AAO wall are negligible (see reference sample in Fig. S2). Therefore, all the molecules are the effective Raman tags experienced large local field. The SERS results imply that field intensity in the gap of the dimer AuNRs is far larger than that of the one-segment AuNRs confined near one end region. Here, using dimer AuNR arrays as SERS substrate has three advantages: 1) the L-SPR of array is determined by the rod-length and then could be easily tuned for excitation or emission resonance; 2) the intense local field in the gap region induces large SERS enhancement; 3) the perfect spatial overlay of the Raman molecules and the hot spots leads to high stability and reproducibility (see Fig. S3). Besides the Au-Au dimer NRs, the Au-Ag dimer NRs (Fig. S4) and the Ag-Ag dimer NRs [49] also exhibits high SERS performance.

The field enhancement in the dimer gap could be tuned by the length ratio L_1/L_2 of two segments. We prepared five two-segment dimer AuNR arrays with different length ratio L_1/L_2, which could be controlled by the deposition time of two steps (Fig. S5). The length ratio L_1/L_2 was set as 1:5, 2:4, 3:3, 4:2 and 5:1, respectively. The overall length was set same and then the L-SPR wavelength was stable (Fig. S6). Figure 2c shows the SERS spectra of five samples. The SERS intensity at 1067 cm^{-1} peak as a function of the length ratio is shown in Figure 2d. It is clear seen that the SERS intensity of dimer NR array with L_1/L_2 = 3:3 shows the highest intensity. The variation of SERS intensity indicates the field enhancement is dependent on the length ratio L_1/L_2, which is consistent with the previous reports [49].

We further demonstrate the existence of a large local field enhancement in the gap of two-segment AuNR arrays by measuring the TPL. As shown in Fig. 3a, with the excitation wavelength of 785 nm and the excitation power P = 140 mW, one-segment and two-segment AuNR arrays exhibit a broadband spectra ranged from 500 nm to 680 nm, which is attributed to the TPL of Au (see then inset of Fig. 3b and Fig. S7). The TPL signal is very weak for the one-segment AuNR arrays, while TPL intensity is enhanced over 11-27 times at the emission wavelength at 672 nm by the two-segment AuNR arrays. The TPL intensity of the peak at λ_{emi} = 672 nm as a function of the length ratio L_1/L_2 is shown in Fig. 3b. The dependence of TPL intensity on the length ratio L_1/L_2 is well consistent with the profile that of Raman intensity in Fig. 2d and the two-segement dimer AuNR array with L_1/L_2 = 3:3 shows the highest TPL intensity. Au nanostructures have been reported to exhibit the strong TPL and TPL is a nonlinear optical process showing more sensitive to the field intensity [64-66]. The observed strong TPL is ascribed to the manifestation of local field enhancement [67-69] and displays a well agreement with the Raman measurement.

Here, the fabrication method and the resulting products provide an interesting pathway to the plasmonic application. The molecular self-assembled monolayer introduces an ultra-narrow gap of ~1 nm in the AuNR dimer and then induces a large field enhancement in the junction for plasmonic antenna. Meanwhile, the molecules also act as Raman tags and the dimer AuNR arrays serve as the fine SERS subtrate. The intrinsic advantage is that the Raman molecules are entirely and accurately located in the gap region and experienced highly confined and enhanced field.

Now, we turn to the observation and understanding of coaxial cable NR arrays. Figure 4a shows the fabrication procedure of Au@Ag core@shell cable NR arrays. After the deposition of AuNRs, the pore widening treatment produced an "air shell" around the AuNR (Fig. S8). Then the 1,4-BDT molecules could be adsorbed and assembled on the uncovered surface of AuNRs including the top end and all side surfaces. The subsequent deposition of Ag filled the "air shell" and produced an array of AuNR core-Ag shell coaxial cable (Fig. S9) [50-53]. Figures 4b and 4c show the top-view SEM images of etch-out bare AuNRs and cable NRs, respectively. It can be seen that the diameter of cable NRs is ~37 nm, which is obviously larger than ~28 nm diameter of the bare AuNRs. The pore widening effect and the deposition of Ag as shells could also be verified the extinction spectra (Fig. S10).

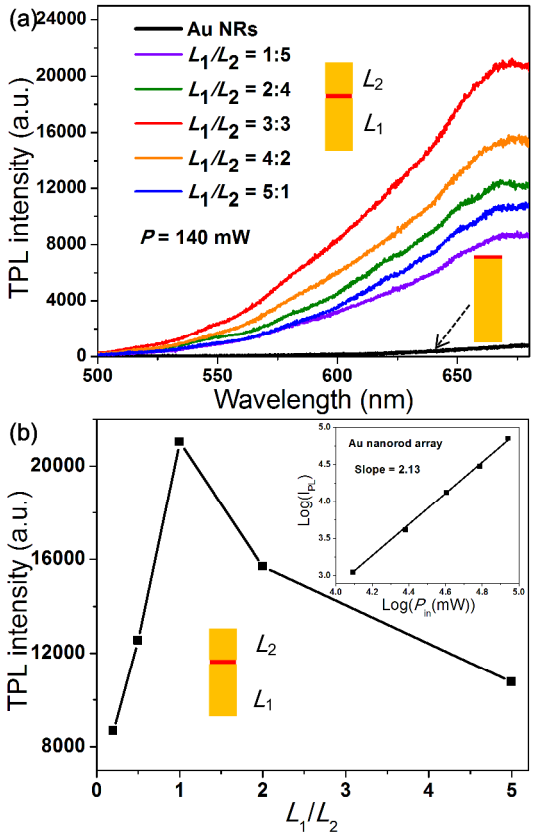

Fig. 3 (a) TPL spectra of five two-segment dimer AuNRs arrays with different length ratio. The length ratio L_1/L_2 is 1:5, 2:4, 3:3, 4:2 and 5:1, respectively. (b) TPL intensity at λ_{emi} = 672 nm as a function of the length ratio L_1/L_2. The inset shows the log-log plot of the luminescence intensity on the excitation power.

The L-SPRs of the bare AuNR array and coaxial cable Au@Ag NR array are set nearly same at ~785 nm and resonant with the Raman excitation (Fig. 5a). For the coaxial cable Au@Ag NR array, the new band at 413 nm is corresponding to the SPR of Ag, and the T-SPR band shows a slight blue-shift from 530 nm to 515 nm due to the silver coating [70,71]. More interesting, the L-SPR extinction intensity is greatly enhanced, which is due to the coupling induced large field enhancement confined in the gap

region between the AuNR core and Ag shell. Similarly as the dimer NR array, Raman molecules adsorbed on the side surface of core AuNRs experience the intense field generated in the gap. As shown in Figure 5b, the SERS signal of cable NR array is enhanced, over 16 times compared with the bare AuNR array, and shows good stability and reproducibility (Fig. S11). Another interesting phenomenon is that the Raman pattern is different for the dimer and cable NR arrays. The strongest peak is changed from 1067 cm^{-1} for Au-Au dimer NRs to 1573 cm^{-1} for Au@Ag cable NRs, and the intensity ratio of 1067 cm^{-1} to the 1556 cm^{-1} changes from 1.318 to 0.959. We also observe the variation of Raman peak position and width in Fig. 2c and Fig. 5d. We attribute these evolutions to the different adsorption configuration of 1,4-BDT molecules on the surface of Au and Ag [57,61] as well as the charge-transfer mechanism [72].

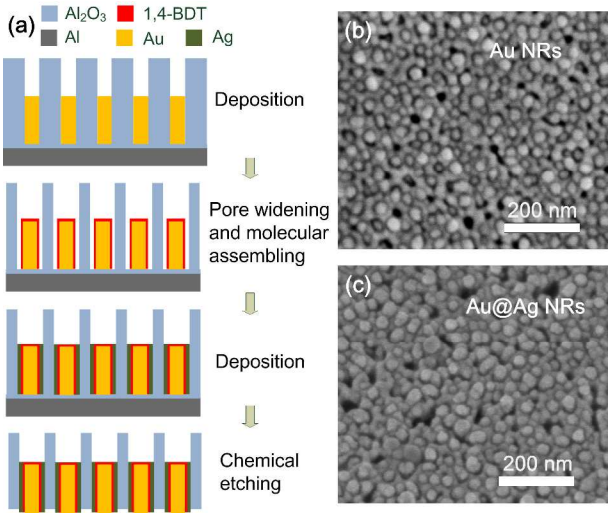

Fig. 4 (a) Schematic illustration for preparing coaxial cable Au@Ag NR arrays. SEM images of (b) etched back-side of a bare AuNRsarray and (c) etched back-side of a coaxial cable Au@Ag NRs array.

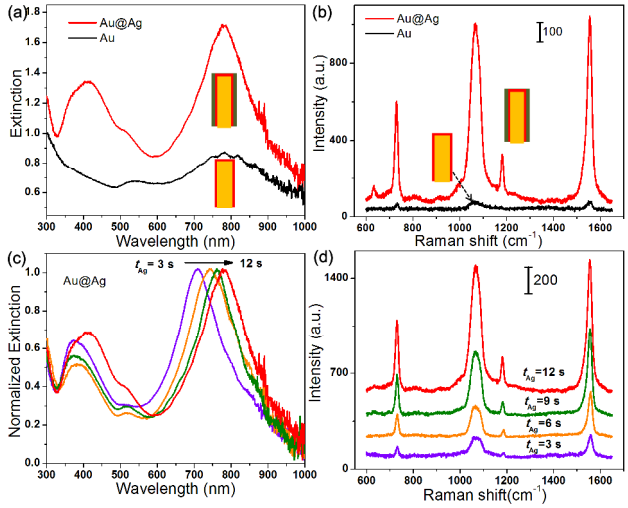

Fig. 5 (a) Extinction and (b) SERS spectra of bare Au NRs and coaxial cable Au@Ag NR arrays with 1,4-BDT molecules adsorbed on the uncovered surface of AuNRs and confined in the junction of coaxial cable Au@Ag NRs. (c) Normalized extinction and (d) SERS spectra of four coaxial cable Au@Ag NR arrays with different deposition time of Ag (t_{Ag}), t_{Ag} = 3 s, 6 s, 9 s and 12 s, respectively.

The L-SPR band and the field enhancement can be tuned by the deposition time of Ag shell. As the extinction spectra shown in Fig. 5c, the L-SPR band red-shifts from 710 nm to 783 nm as the deposition time of Ag increases from 3 s to 12 s. It should be noted that, for the sample with the Ag deposition time of 12 s, the Ag palsmon band near 400 nm red-shifts obviously, which possibly implies the "air shell" is fully filled in vertical by the Ag shell. The Raman signal intensity increases with the deposition time of Ag (Fig. 5d) , which could be ascribed to two factors: 1) the red-shifted L-SPR band is more near the Raman excitation of 785 nm; 2) as Ag grows in vertical and fills the air shells, more Raman molecules are packaged into the gap region.

The local field confinements and enhancements of two-segment dimer and coaxial cable NR arrays are revealed by using 3D finite-difference time domain (FDTD) simulations. Figure 6 shows that the local field distributions of AuNR, two-segment dimer Au-Au NR and coaxial cabel Au@Ag NR arrays. It can be seen the field is greatly confined and enhanced in the gap region for dimer and cable NRs.

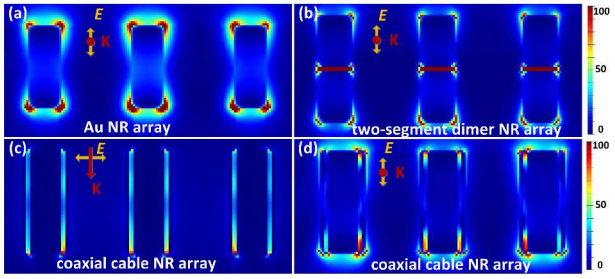

Fig. 6 FDTD simulations of local field distribution. (a) AuNR array, (b) Au-Au two-segment dimer NR array, (c) and (d) Au@Ag coaxial cable NR array. The directions of wave vector and polarization are marked.

4. Conclusions

In summary, plasmonic arrays of two-segment dimer Au-Au NRs and coaxial cable Au@Ag NRs with ~1 nm gap insulated by self-assembled Raman molecule monolayer have been fabricated by a two-step electrodeposition method. The gap-induced plasmon coupling generates intense field in the gap region of dimer junction and cable interlayer. Hence, the L-SPRs of NR arrays are greatly enhanced and show high tunability. The field enhancement can be tuned by the length ratio of two segments for the dimer NR arrays and the deposition time of Ag shells for the cable NR arrays. Furthermore, the TPL and Raman scattering under resonant excitation are investigated to reveal the nature of plasmon induced field enhancement. As a nonlinear optical process showing more sensitive to the field intensity, the TPL of dimer NR arrays is enhanced by 27 times comparing with the bare AuNR arrays. Causing the intrinsic advantage that the Raman molecules are all accurate placed in the gap region, the SERS is enhanced by 30 times and 16 times for the dimer NR arrays and the cable NR arrays, respectively, and exhibits excellent performance with high sensitivity, reproducibility, and tunability. The studies in this paper have potential to be used as functional meta-materials, nano-antenna for manipulating light emission, and reliable quantitative SERS device in bio-application.

Acknowledgements

The authors gratefully acknowledge the Center for Elector Microscopy of Wuhan University, in particular Mr. Qiang Fu, Mr. Mr. Jiahong Wang, and Mr. Hao Huang, for providing support of SEM, Raman measurements. This work was supported in part by the National Program on Key Science Research of China (2011CB922201), and the NSFC (11174229, 11204221 and 11374236).

Notes and references

[a]*Key Laboratory of Artificial Micro- and Nano-structures of the Ministry of Education, and School of Physics and Technology, Wuhan University, Wuhan, 430072, P.R.China;* [b]*Institute for Advanced Study, Wuhan University, Wuhan 430072, P. R. China. Electronic mail: qqwang@whu.edu.cn; zhouli@whu.edu.cn.*

† Electronic Supplementary Information (ESI) available: [details of any supplementary information available should be included here]. See DOI: 10.1039/b000000x/

1 A. V. Kabashin, P. Evans, S. Pastkovsky, W. Hendren, G. A. Wurtz, R. Atkinson, R. Pollard, V. A. Podolskiy and A. V. Zayats, *Nat. Mater.*, 2009,**8**, 867-871.
2 T. A. Taton, C. A. Mirkin, and R. L. Letsinger, *Science*, 2000,**289**, 1757-1760.
3 J. J. Storhoff, A. D. Lucas, V. Garimella, Y. P. Bao and U. R. Muller, *Nat. Biotechnol.*, 2004,**22**, 883-887.
4 R. Elghanian, J. J. Storhoff, R. C. Mucic, R. L. Letsinger, and C. A. Mirkin, *Science*, 1997,**277**, 1078-1081.
5 S. V. Boriskina and B. M. Reinhard, *Proc. Natl. Acad. Sci. USA*, 2011,**108**, 3147-3151.
6 D. J. Bergman and M. Stockman, *Phys. Rev. Lett.*, 2003, **90**, 027402.
7 J. A. Schuller, E. S. Barnard, W. Cai, Y. C. Jun, J. S. White and M. L. Brongersma, *Nat. Mater.*, 2010,**9**, 193-204.
8 H. T. Miyazaki and Y. Kurokawa, *Phys. Rev. Lett.*, 2006, **96**, 097401.
9 K. L. Kelly, E. Coronado, L. L. Zhao and G. C. Schatz, *J. Phys. Chem. B*, 2003,**107**, 668-677.
10 J. Zhang, H. Liu, Z. Wang and N. Ming, *Adv. Funct. Mater.*, 2007,**17**, 3295-3303.
11 X. Duan, Y. Huang, Y. Cui, J. Wang and C. M. Lieber, *Nature*, 2001,**409**, 66-69.
12 S. Nie, and S. R. Emory , *Science*, 1997,**275**, 1102-1106.
13 K. Kneipp, Y. Wang, H. Kneipp, L. Perelman, I. Itzkan, R. Dasari and M. Feld, *Phys. Rev. Lett.*, 1997,**78**, 1667-1670.
14 K. Kneipp, H. Kneipp and J. Kneipp, *Acc. Chem. Res.*, 2006,**39**, 443-450.
15 R. F. Oulton, V. J. Sorger, T. Zentgraf, R. M. Ma, C. Gladden, L. Dai, G. Bartal and X. Zhang, *Nature*, 2009,**461**, 629-632.
16 R. M. Ma, R. F. Oulton, V. J. Sorger, G. Bartal and X. Zhang, *Nat. Mater.*, 2011,**10**, 110-113.
17 Y. J. Lu, J. Kim, H. Y. Chen, C. Wu, N. Dabidian, C. E. Sanders, C. Y. Wang, M. Y. Lu, B. H. Li, X. Qiu, W. H. Chang, L. J. Chen, G. Shvets, C. K. Shih and S. Gwo, *Science*, 2012,**337**, 450-453.
18 H. Liang, Z. Li, W. Wang, Y. Wu and H. Xu, *Adv. Mater.*, 2009,**21**, 4614-4618.
19 J. Lee, B. Hua, S. Park, M. Ha, Y. Lee, Z. Fan and H. Ko, *Nanoscale*, 2014,**6**, 616-623.
20 F. Hao, C. L. Nehl, J. H. Hafner and P. Nordlander, *Nano Lett.*, 2007,**7**, 729-732.
21 H. Ko, S. Chang and V. V. Tsukruk, *ACS Nano*, 2009,**3**, 181-188.
22 C. Oubre and P. Nordlander, *J. Phys .Chem. B*, 2005,**109**, 10042-10051.
23 D. K. Lim, K. S. Jeon, J. H. Hwang, H. Kim, S. Kwon, Y. D. Suh and J. M. Nam, *Nat. Nanotechnol.*, 2011,**6**, 452-460.
24 H. H. Wang, C. Y. Liu, S. B. Wu, N. W. Liu, C. Y. Peng, T. H. Chan, C. F. Hsu, J. K. Wang and Y. L. Wang, *Adv. Mater.*, 2006, **18**, 491–495
25 S. J. Lee, Z. Guan, H. Xu and M. Moskovits, *J. Phys. Chem. C*, 2007,**111**, 17985-17988.
26 Z. Q. Tian, B. Ren and D. Y. Wu, *J. Phys .Chem. B*, 2002,**106**, 9463-9483.
27 Z. Dai, X. Xiao, L. Liao, J. Zheng, F. Mei, W. Wu, J. Ying, F. Ren and C. Jiang, *Appl. Phys. Lett.* , 2013, 103, 041903.
28 N. A. Hatab, C. H. Hsueh, A. L. Gaddis, S. T. Retterer, J. H. Li, G. Eres, Z. Zhang and B. Gu, *Nano Lett.*, 2010,**10**, 4952-4955.
29 Y. Chu, M. G. Banaee and K. B. Crozier, *ACS Nano*, 2010,**4**, 2804-2810.
30 T. Atay, J. H. Song and A. V. Nurmikko, *Nano Lett.*, 2004,**4**, 1627-1631.
31 K. H. Su, Q. H. Wei, X. Zhang, J. J. Mock, D. R. Smith and S. Schultz, *Nano Lett.*, 2003,**3**, 1087-1090.
32 Y. Lu, G. L. Liu and L. P. Lee, *Nano Lett.*, 2005,**5**, 5-9.
33 H. Liu, Z. Yang, L. Meng, Y. Sun, J. Wang, L. Yang, J. Liu and Z. Tian, *J. Am. Chem. Soc.*, 2014,**136**, 5332-5341.
34 W. Dickson, G. Wurtz, P. Evans, D. O'Connor, R. Atkinson, R. Pollard and A. Zayats, *Phys. Rev. B*, 2007,**76**, 115411.
35 R. Atkinson, W. Hendren, G. Wurtz, W. Dickson, A. Zayats, P. Evans and R. Pollard, *Phys. Rev. B*, 2006,**73**. 235402
36 P. R. Evans, G. A. Wurtz, R. Atkinson, W. Hendren, D. O'Connor, W. Dickson, R. J. Pollard and A. V. Zayats, *J. Phys. Chem. C*., 2007,**111**, 12522-12527.
37 S. J. Lee, A. R. Morrill and M. Moskovits, *J. Am. Chem. Soc.*, 2006,**128**, 2200-2201.
38 Z. Huang, G. Meng, Q. Huang, Y. Yang, C. Zhu and C. Tang, *Adv. Mater.*, 2010,**22**, 4136-4139.
39 J. F. Li, Y. F. Huang, Y. Ding, Z. L. Yang, S. B. Li, X. S. Zhou, F. R. Fan, W. Zhang, Z. Y. Zhou, Y. Wu de, B. Ren, Z. L. Wang and Z. Q. Tian, *Nature*, 2010,**464**, 392-395.
40 P. Johansson, H. Xu and M. Käll, *Phys. Rev. B*, 2005,**72**. 035427.
41 K. Okamoto, I. Niki, A. Shvartser, Y. Narukawa, T. Mukai and A. Scherer, *Nat. Mater.*, 2004,**3**, 601-605.
42 F. Nan, Z. Q. Cheng, Y. L. Wang, Q. Zhang, L. Zhou, Z. J. Yang, Y. T. Zhong, S. Liang, Q. H. Xiong and Q. Q. Wang, *Sci. Rep.*, 2014,**4**, 4839.
43 J. Kumar, R. Thomas, R. S. Swathi and K. G. Thomas, *Nanoscale*, 2014,**6**, 10454-10459.
44 P. H. Camargo, M. Rycenga, L. Au and Y. Xia, *Angew. Chem. Int. Ed.*, 2009,**48**, 2180-2184.
45 Ye, J. A. Hutchison, H. Uji-i, J. Hofkens, L. Lagae, G. Maes, G. Borghs and P. Van Dorpe, *Nanoscale*, 2012,**4**, 1606-1611.
46 E. Dujardin, S. Mann, L. B. Hsin and C. R. C. Wang, *Chem. Commun.*, 2001, **427**, 1264-1265.
47 A. Barhoumi, D. Zhang, F. Tam and N. J. Halas, *J. Am. Chem. Soc.*, 2008,**130**, 5523-5529.
48 X. Zhao, G. Meng, Q. Xu, F. Han and Q. Huang, *Adv. Mater.*, 2010,**22**, 2637-2641.
49 G. H. Gu and J. S. Suh, *Langmuir*, 2008,**24**, 8934-8938.
50 P. R. Evans, W. R. Hendren, R. Atkinson and R. J. Pollard, *J. Electrochem. Soc.*, 2007,**154**, K79.
51 P. R. Evans, W. R. Hendren, R. Atkinson and R. J. Pollard, *Nanotechnology*, 2008,**19**, 465708.
52 A. Murphy, Y. Sonnefraud, A. V. Krasavin, P. Ginzburg, F. Morgan, J. McPhillips, G. Wurtz, S. A. Maier, A. V. Zayats and R. Pollard, *Appl. Phys. Lett.*, 2013,**102**, 103103.
53 M. Lahav, E. A. Weiss, Q. Xu and G. M. Whitesides, *Nano Lett.*, 2006,**6**, 2166-2171.
54 Johnson P B, Christy R W, *Phys. Rev. B*, 1972, **6**, 4370–4379.
55 E. D. Palik, *Handbook of Optical Constants of Solids*, Academic Press, New York, 1985.
56 W. Lee, J. C. Kim and U. Gösele, *Adv. Funct. Mater.*, 2010,**20**, 21-27.
57 R. B. Pontes, F. D. Novaes, A. Fazzio and A. J. da Silva, *J. Am. Chem. Soc.*, 2006,**128**, 8996-8997.
58 J. Jiang, K. Bosnick, M. Maillard and L. Brus, *J. Phys. Chem. B*, 2003,**107**, 9964–9972.
59 G. H. Gu, J. Kim, L. Kim and J. S. Suh, *J. Phys. Chem. C*, 2007, **111**, 7906-7909.
60 S. H. Cho, H. S. Han, D. J. Jang, K. Kim and M. S. Kim, *J. Phys. Chem. C*, 1995,**99**, 10594-10599.
61 S. W. Joo, S. W. Han and K. Kim, *J. Colloid. Interface. Sci.*, 2001,**240**, 391-399.
62 J. M. McLellan, A. Siekkinen, J. Chen and Y. Xia, *Chem. Phys. Lett.*, 2006,**427**, 122-126.

63 P. H. Camargo, C. M. Cobley, M. Rycenga and Y. Xia, *Nanotechnology*, 2009,**20**, 434020.

64 X. L. Liu, S. Liang, F. Nan, Z. J. Yang, X. F. Yu, L. Zhou, Z. H. Hao and Q. Q. Wang, *Nanoscale*, 2013,**5**, 5368-5374.

65 T. Zhao, X. Shen, L. Li, Z. Guan, N. Gao, P. Yuan, S. Q. Yao, Q. H. Xu and G. Q. Xu, *Nanoscale*, 2012,**4**, 7712-7719.

66 Z. Guan, N. Gao, X. F. Jiang, P. Yuan, F. Han and Q. H. Xu, *J. Am. Chem. Soc.*, 2013,**135**, 7272-7277.

67 P. Muhlschlegel, H. J. Eisler, O. J. Martin, B. Hecht and D. W. Pohl, *Science*, 2005,**308**, 1607-1609.

68 A. Bouhelier, R. Bachelot, G. Lerondel, S. Kostcheev, P. Royer and G. P. Wiederrecht, *Phys. Rev. Lett.*, 2005,**95**, 267405.

69 P. J. Schuck, D. P. Fromm, A. Sundaramurthy, G. S. Kino and W. E. Moerner, *Phys. Rev. Lett.*, 2005,**94**, 017402.

70 S. Pande, S. K. Ghosh, S. Praharaj, S. Panigrahi, S. Basu, S. Jana, A. Pal, T. Tsukuda and T. Pal, *J. Phys. Chem. C*, 2007,**111**, 10806-10813.

71 Y. Yang, J. Shi, G. Kawamura, and M. Nogami, *Scripta Mater.*, 2008, **58**, 862-865.

72 S. Pande, J. Chowdhury and T. Pal, *J. Phys. Chem. C*, 2011, **115**, 10497-10509.